

# Structural Polymorphism Exhibited by Polyglycidol-Based Analogues to *Pluronic* Copolymers in Aqueous Solution

Stanislav Rangelov,<sup>\*,†</sup> Silvia Halacheva,<sup>†,‡</sup> Vasil M. Garamus,<sup>§</sup> and Mats Almgren<sup>||</sup>

*Institute of Polymers, Bulgarian Academy of Sciences, Acad. G. Bonchev 103-A, 1113 Sofia, Bulgaria, Department of Chemistry, University of Bath, Claverton Down, Bath, BA2 7AY, United Kingdom, GKSS Research Centre, Max-Planck Strasse 1, D-21502 Geesthacht, Germany, and Department of Physical and Analytical Chemistry, University of Uppsala, Uppsala, Sweden*

Received June 3, 2008; Revised Manuscript Received September 25, 2008

**ABSTRACT:** In this paper, nanostructures formed in water by a novel series of  $(G)_n(PO)_{68}(G)_n$  triblock copolymers, where  $n = 18–135$ , and G and PO stand for glycidol and propylene oxide, respectively, are parametrized. The copolymers are considered analogues of *Pluronic* copolymers in which the flanking poly(ethylene oxide) (PEO) blocks are substituted by polyglycidol (PG). PG is structurally similar to PEO and differs in that each monomer unit bears a hydroxymethylene group. In composition, the copolymers are closest to the *Pluronic* series L121–F127. Dilute (but invariably above the critical aggregation concentration) aqueous solutions in the temperature interval 25–70 °C were investigated by means of dynamic and static light scattering, cryogenic transmission electron microscopy, and small-angle neutron scattering (SANS). In the temperature-composition continuum studied the novel copolymers exhibit rich structural polymorphism. Large compound particles as those observed earlier for related copolymers, small core-corona micelles, rods, and vesicles were detected and parametrized by combining light scattering and SANS. Upon heating, the simultaneous increase in both hydrophobicity of poly(propylene oxide) and hydrophilicity of PG cause counteracting effects that are reflected in appearance of maxima in the temperature dependence of aggregation numbers of the particles, variations in the density of the latter, and anomalous thermotropic transitions for some of the copolymers.

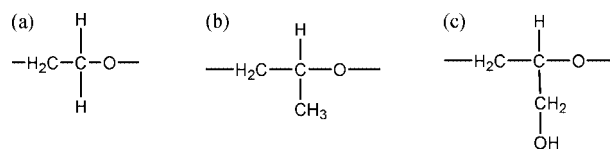
## Introduction

One class of nonionic macromolecular surfactants that have attracted a great interest from both industry and academia are the poly(alkylene oxide) block copolymers. Among them poly(ethylene oxide)-poly(propylene oxide)-poly(ethylene oxide), PEO-PPO-PEO, are commercially available (commonly known under the trade name *Pluronic*) in a wide range of compositions. In a more limited composition range, ethylene oxide/propylene oxide (EO/PO) as well as ethylene oxide/butylene oxide (EO/BO) block copolymers of diblock, reverse triblock, and star-like architectures have been commercialized or prepared in laboratory scales and quantities. The interest in these groups of copolymers reflects their both widespread applications and intriguing self-association in selective solvents, water in particular. Presently, much is known about them; they have been extensively studied by a number of research groups and techniques, including scattering methods and transmission electron microscopy. Reviews<sup>1</sup> that periodically appeared carry extensive lists of references. Basically, the copolymers self-associate to form a variety of dispersed nanostructures (spherical micelles, rods, vesicles) and liquid-crystalline phases (cubic, hexagonal, lamellar), depending on the copolymer composition, solution concentration, and temperature. All basic particle morphologies and liquid-crystalline phases have been observed and documented. In these nanostructures and phases, the hydrophobic PPO (or PBO) chains<sup>2</sup> are sequestered in domains of a certain shape, whereas the hydrophilic PEO chains interact with the aqueous phase.

To add to the accumulated knowledge, a series of copolymers that can be considered as analogues to *Pluronic* copolymers in

which the flanking PEO blocks are substituted with blocks of structurally similar linear polyglycidol (PG) has recently been prepared.<sup>3a</sup> This series was based nominally on PPO of molecular weight of 2000, that is, the copolymers are closest in composition to the *Pluronic* series L61–F68 and L72–F77. It is intriguing that a seemingly small chemical modification of the hydrophilic block (see Figure 1 for the chemical structures of the monomer units) manifests itself in large differences in the self-assembly, dimensions, and structures of the aggregates compared to those of *Pluronic* copolymers.<sup>3b,c</sup> Hydrophobic interactions and interactions via hydrogen bonding are equally involved in formation of large compound particles with discontinuous PPO domains randomly distributed in a strongly hydrogen-bonded continuous medium containing PG and water.<sup>3b</sup> The particles are considerably larger in size (above 60 nm in radius) and aggregation number (above 100) than the micelles of the *Pluronic* copolymers. A recent small-angle neutron scattering (SANS) study<sup>3c</sup> revealed that in the interior of the large compound particles PPO domains of slightly prolate spherical shape coexisted with individual copolymer chains that mediated interdomain interactions via hydrogen bonding rather than to participate in the formation of the PPO domains.

Following a recent paper on synthesis and preliminary aqueous solution properties of a novel series<sup>4</sup> of PG-based analogues to *Pluronic* copolymers, this paper continues the earlier research. The present PG-PPO-PG triblock copolymers are nominally based on PPO of molecular weight of 4000, which makes them closest in composition to the *Pluronic* series



**Figure 1.** Monomer units of (a) poly(ethylene oxide), (b) poly(propylene oxide), and (c) linear polyglycidol.

\* To whom correspondence should be addressed. Tel.: +359 2 9792293. Fax: +359 2 8700309. E-mail: rangelov@polymer.bas.bg.

<sup>†</sup> Bulgarian Academy of Sciences.

<sup>‡</sup> University of Bath.

<sup>§</sup> GKSS Research Centre.

<sup>||</sup> University of Uppsala.

**Table 1. Polyglycidol Content, Composition, Total Copolymer Molecular Weight, and Codes of the Copolymers Used in This Study**

| PG content (wt %) | composition  | total molecular weight | code   |
|-------------------|--|------------------------|--------|
| 40                | (G) <sub>18</sub> (PO) <sub>68</sub> (G) <sub>18</sub>   | 6700                   | LGP134 |
| 50                | (G) <sub>27</sub> (PO) <sub>68</sub> (G) <sub>27</sub>   | 8000                   | LGP135 |
| 60                | (G) <sub>40</sub> (PO) <sub>68</sub> (G) <sub>40</sub>   | 9900                   | LGP136 |
| 70                | (G) <sub>63</sub> (PO) <sub>68</sub> (G) <sub>63</sub>   | 13300                  | LGP137 |
| 80                | (G) <sub>135</sub> (PO) <sub>68</sub> (G) <sub>135</sub> | 24000                  | LGP138 |

L121–F127. Using scattering methods, in particular, dynamic (DLS), static (SLS) light scattering, and SANS, as well as cryogenic transmission electron microscopy (cryo-TEM), the self-assembled structures formed in water by the novel series of copolymers (see Table 1 for the PG content, composition, copolymer molecular weight, and codes of the copolymers) are parametrized in wide composition and temperature ranges. The present copolymers exhibit structural polymorphism, thermotropic transitions, and variations in particle parameters that have not been observed for the previous series of related copolymers.<sup>3b,c</sup>

## Experimental Section

**A. Materials.** The copolymers used in the present study were synthesized as described elsewhere.<sup>4</sup> They are symmetric linear triblock copolymers of a general formula (G)<sub>n</sub>(PO)<sub>68</sub>(G)<sub>n</sub>, where G and PO denote glycidol and propylene oxide units, respectively, and *n* varies from 18 to 135. The composition, polyglycidol content, total molecular weight, and the codes of the copolymers are given in Table 1.

**B. Sample Preparation.** Aqueous solutions in the concentration range from 0.298 to 9.95 mg·mL<sup>-1</sup> were prepared by dilution of stock solutions. The latter were prepared gravimetrically by adding water to preweighted quantity of the copolymer and allowed to mix overnight by shaking occasionally. Then additional amount of water was added to get solutions of desired concentration. D<sub>2</sub>O (Aldrich) with D purity higher than 99.8% was used to prepare solutions for the SANS measurements. The solutions were prepared gravimetrically.

**C. Methods. Light Scattering.** The light scattering setup has been described previously.<sup>5</sup> It consists of a 632.8 nm He/Ne laser and the detector optics with an ITT FW 130 photomultiplier and ALV-PM-PD amplifier-discriminator connected to an ALV-5000 auto-correlator built into a computer. The cylindrical scattering cells were sealed and then immersed in a large-diameter thermostatted bath containing the index matching fluid decalin. Measurements were made at different angles in the range of 50–130° and at different temperatures. Analysis of the dynamic data was performed by fitting the experimentally measured *g*<sub>2</sub>(*t*), the normalized intensity auto-correlation function, which is related to the electrical field correlation function *g*<sub>1</sub>(*t*) by the Siegert relationship<sup>6</sup>

$$g_2(t) - 1 = \beta |g_1(t)|^2 \quad (1)$$

where  $\beta$  is a factor accounting for deviation from ideal correlation. For polydisperse samples, *g*<sub>1</sub>(*t*) can be written as the inverse Laplace transform (ILT) of the relaxation time distribution,  $\tau A(\tau)$

$$g_1(t) = \int A(\tau) \exp(-t/\tau) d \ln \tau \quad (2)$$

where  $\tau$  is the lag-time. The relaxation time distribution,  $\tau A(\tau)$  was obtained by performing ILT using the constrained regularization algorithm REPES, which minimizes the sum of the squared differences between the experimental and the calculated *g*<sub>2</sub>(*t*).<sup>7</sup> A mean diffusion coefficient *D* was calculated from the position of each peak as  $D = \Gamma/q^2$ , where *q* is the magnitude of the scattering vector  $q = (4\pi n/\lambda) \sin(\theta/2)$  and  $\Gamma = 1/\tau$  is the relaxation rate of each mode. Here,  $\theta$  is the scattering angle, *n* is the refractive index of the medium, and  $\lambda$  is the wavelength of the light in vacuum.

Within the dilute regime *D* varies linearly with the concentration according to

$$D = D_0(1 + k_D C + \dots) \quad (3)$$

where *D*<sub>0</sub> is the diffusion coefficient at infinite dilution and *k*<sub>D</sub> is the hydrodynamic virial coefficient. The Stokes–Einstein equation relates *D*<sub>0</sub> and the hydrodynamic radius, *R*<sub>h</sub>

$$R_h = kT/(6\pi\eta D_0) \quad (4)$$

Here, *kT* is the thermal energy factor and  $\eta$  is the temperature-dependent viscosity of the solvent.

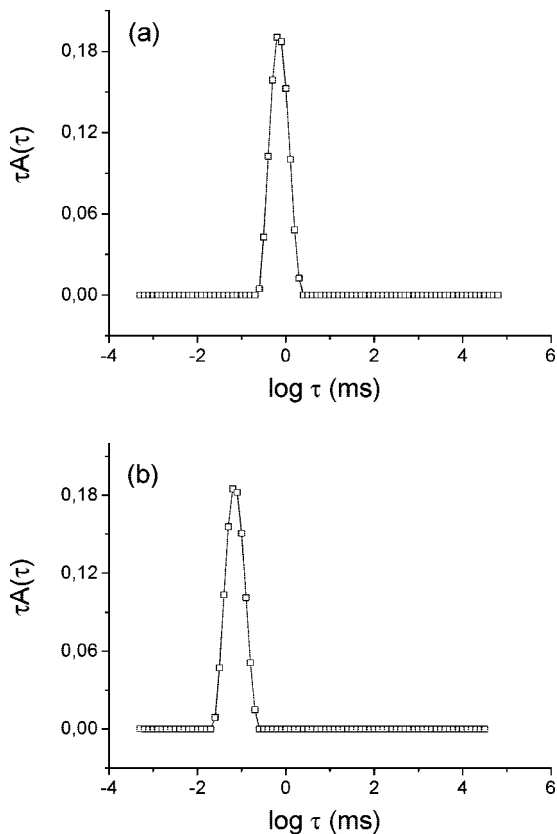
SLS was performed with samples exhibiting monomodal relaxation time distribution from DLS. Information on the weight-average molar masses, *M*<sub>w</sub>, the radii of gyration, *R*<sub>g</sub>, and the second virial coefficients, *A*<sub>2</sub>, was typically obtained from the static light scattering data using the Zimm plot method. The angular dependence of the reduced scattered light intensity, *Kc/R*<sub>θ</sub>, of the copolymer solutions was measured in the static experiments. Here,  $K = 4\pi^2 n^2 (dn/dc)^2 / N_A \lambda^4$ , *N*<sub>A</sub> is Avogadro's constant, and  $\lambda$  is the wavelength of the light in a vacuum. The refractive index increment, *dn/dc*, was measured in a differential refractometer with Rayleigh optics. For the present systems, *dn/dc* values were in the 0.104–0.137 mL·g<sup>-1</sup> range at the wavelength used; they were found to decrease with increasing temperature with temperature coefficients from  $-1.27 \times 10^{-4}$  to  $-2.51 \times 10^{-4}$  mL·g<sup>-1</sup>·K<sup>-1</sup>, depending on the copolymer composition. *R*<sub>θ</sub> is the Rayleigh ratio at a given angle ( $\theta$ ). The reduced scattered light intensity was linearly dependent on  $\sin^2(\theta/2)$ , indicating that the angle range was appropriately chosen. All static parameters were derived by extrapolation to zero micellar concentration.

**Cryogenic Transmission Electron Microscopy (cryo-TEM).** Transmission electron microscopy observations were conducted on a Zeiss EM 902 A instrument operating at 80 kV. The procedure for the sample preparation is described in the following. A drop of the dispersion is deposited on an electron microscopy copper grid coated by a perforated polymer film. The excess of the liquid is blotted by a filter paper leaving a thin film of the dispersion on the grid. The film on the grid is vitrified by plunging the grid into liquid ethane. The vitrified sample is then transferred to the microscope for observation close to liquid nitrogen temperature.

**Small-Angle Neutron Scattering.** The SANS experiments were performed at the SANS1 instrument at the FRG1 research reactor at GKSS Research Centre, Geesthacht, Germany.<sup>8</sup> The range of scattering vectors *q* from 0.005 to 0.26 Å<sup>-1</sup> was covered by four sample-to-detector distances (from 0.7 to 9.7 m). The neutron wavelength was 8.1 Å, and the wavelength spread of the mechanical velocity selector was 10% (fwhm). The samples were kept in quartz cells (Helma, Germany) with a path length of 2 mm. For isothermal conditions, a thermostatted sample holder was used. The raw spectra were corrected for backgrounds from the solvent, sample cell, and other sources by conventional procedures. The two-dimensional isotropic scattering spectra were azimuthally averaged, converted to absolute scale, and corrected for detector efficiency by dividing by the incoherent scattering spectrum of pure water, which was measured with a 2 mm path length quartz cell. The smearing induced by the different instrumental settings was included in the data analysis.<sup>9</sup>

## Results and Discussion

**Light Scattering Experiments.** In aqueous surrounding and above the critical aggregation concentration (CAC) the copolymers typically exhibit bimodal relaxation time distributions (see Supporting Information for a representative distribution) with a slowly relaxing diffusive component of relative scattered light intensity up to 30% and a hydrodynamic radius in excess of 150 nm. These might be attributable to the presence of large compound particles as those described earlier for related copolymers.<sup>3b,c</sup> However, in strong contrast to the latter, the large compound particles are not the dominant species: a coarse estimate gives *C*<sub>slow</sub>/*C*<sub>dominant</sub> ≤ 10<sup>-1</sup>. Following filtration through 0.2 μm filters the slow moving particles were removed and monomodal relaxation time distributions were manifested

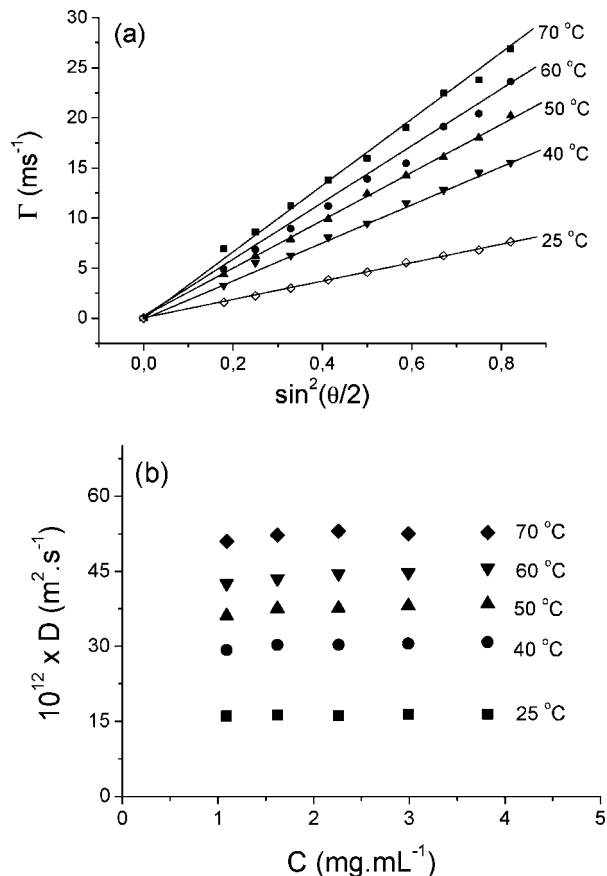


**Figure 2.** Relaxation time distributions measured at an angle of  $90^\circ$  for aqueous solutions of (a) LGP134 at  $c = 0.298 \text{ mg}\cdot\text{mL}^{-1}$  and  $25^\circ\text{C}$  and (b) LGP137 at  $c = 1.62 \text{ mg}\cdot\text{mL}^{-1}$  and  $60^\circ\text{C}$ .

for all copolymers in the investigated concentration and temperature ranges. Representative relaxation time distribution spectra are shown in Figure 2. All peaks were shown to be diffusive: the relaxation rates presented in Figure 3a for LGP138 at  $c = 9.95 \text{ mg}\cdot\text{mL}^{-1}$  and different temperatures showed a linear dependence on  $\sin^2(\theta/2)$  passing through the origin, which indicated diffusive processes. The diffusion coefficients were determined as slopes of the linear fits and then plotted versus concentration (Figure 3b) to get the diffusion coefficient at infinite dilution,  $D_0$ , which were used in the equation of Stokes–Einstein (eq 4) to calculate the hydrodynamic radii. The latter are summarized in Table 2. In striking difference from related copolymers,<sup>3b</sup> the copolymers of the present series form particles considerably smaller in size. At all temperatures the particle dimensions went through a maximum centered at 50 wt % of PG content (LGP135). This phenomenon, which has been repeatedly observed for three independent groups of related PG-based copolymers significantly differing in molecular weight,<sup>3b,10</sup> implies that the PG content of 50 wt % is critical. Indeed, as shown elsewhere,<sup>3,4,10</sup> the aqueous solution properties of the copolymers at this particular PG content sharply changed.

The temperature variations of  $R_h$  are considerably less pronounced compared to those previously reported.<sup>3b</sup> Practically no changes were observed for LGP134 (Table 2). Following a slight collapse, the particles formed by the copolymers of the highest PG contents (LGP137 and LGP138) did not change their dimensions in wide temperature intervals. The low-temperature collapse is somewhat larger and more pronounced for LGP135, whereas the dimensions of the particles formed by LGP136 are constant in the lower ( $25$ – $50^\circ\text{C}$ ) temperature range and upon further heating an approximate 2-fold increase was registered.

With the exception of LGP134 and LGP135, as well as LGP136, at the highest temperatures, the hydrodynamic radii



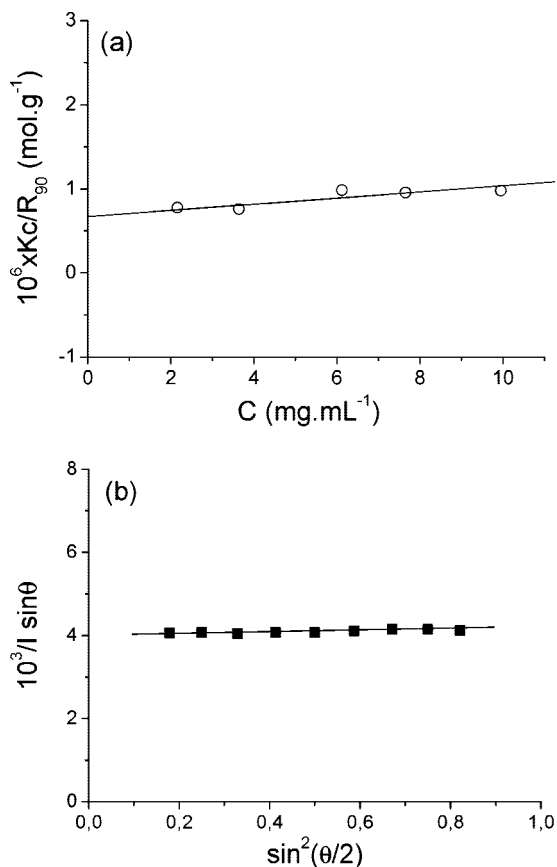
**Figure 3.** (a) Relaxation rate,  $\Gamma$ , as a function of  $\sin^2(\theta/2)$  for LGP138 at  $c = 9.95 \text{ mg}\cdot\text{mL}^{-1}$  and different temperatures. (b) Concentration dependence of diffusion coefficients for LGP137 at different temperatures. The lines through the data points in (a) represent the linear fits to the data.

**Table 2.** Variations of the Hydrodynamic Radii,  $R_h$  (in nm), with Temperature for the Copolymers Studied in Water

|        | $25^\circ\text{C}$ | $40^\circ\text{C}$ | $50^\circ\text{C}$ | $60^\circ\text{C}$ | $70^\circ\text{C}$ |
|--------|--------------------|--------------------|--------------------|--------------------|--------------------|
| LGP134 | 28.0               | 28.2               | 29.3               | 28.9               | 27.9               |
| LGP135 | 54.6               | 38.2               | 38.4               | 38.5               | 33.7               |
| LGP136 | 14.4               | 13.3               | 13.5               | 23.5               | 32.1               |
| LGP137 | 15.3               | 12.1               | 11.3               | 11.7               | 11.7               |
| LGP138 | 18.8               | 12.8               | 13.1               | 14.0               | 13.5               |

reported in Table 2 are in the low nm scale. As the particles are small relative to the wavelength, no angular dependence of the scattered light intensity was found. Thus, the weight-average molar masses,  $M_w$ , and the second virial coefficients,  $A_2$ , were determined from the dependence of the reduced scattered light intensity at  $\theta = 90^\circ$ ,  $Kc/R_{90}$ , versus the copolymer concentration. A representative plot is shown in Figure 4a and the derived static light scattering parameters are summarized in Table 3. For small particles the angular dependence of the quantity  $1/I\sin\theta$  may be useful to estimate the apparent radius of gyration,  $R_g^{\text{app}}$  (Figure 4b). The Zimm plot method was used for the evaluation of the static light scattering parameters of the systems that form larger particles. A typical Zimm plot is presented in Figure 5 and the derived parameters are collected in Table 3. The  $R_g$  variations with temperature are identical to those of  $R_h$ . Thus, the ratio  $R_g/R_h$  is in the range 1.02–1.88, which is compatible with hairy micelles.<sup>11</sup> For the aggregates of LGP136, however, larger values of  $R_g$  were obtained, which gave rise to  $R_g/R_h$  well above 2, implying formation of anisotropic, elongated particles. The magnitude of  $A_2$  is indicative for the strength of the interactions. For the present aggregates they are typically an order of magnitude lower than those of corresponding





**Figure 4.** (a) Reduced scattered light intensity,  $Kc/R_{90}$ , as a function of the concentration of LGP138 at 50 °C. (b) Partial Zimm plot for LGP137 at 60 °C and concentration of 3.82 mg·mL<sup>-1</sup>. The lines through the data points represent the linear fits to the data.

*Pluronic* copolymers, being negative for the copolymers of lower PG content (LGP134 and LGP135) and mostly positive for the copolymers of PG content  $\geq 60$  wt %. The values of  $A_2$  at 25 °C for LGP134 and LGP135, however, as well as that for LGP138 at 70 °C are somewhat erratic. The larger  $A_2$  values for LGP136 should be noted as well.

The aggregation numbers,  $N_{\text{agg}}$ , can be estimated from the  $M_w$  values in Table 3 and molecular weight data of the unimers (Table 1). The variations of  $N_{\text{agg}}$  with temperature are plotted in Figure 6. In contrast to  $R_h$  and  $R_g$ , which were shown to be mostly independent of temperature,  $N_{\text{agg}}$  exhibits pronounced temperature dependence. From the present copolymers only  $N_{\text{agg}}$  of LGP135 decreases with increasing temperature (Figure 6a), which was the rule for related copolymers.<sup>3b</sup> Furthermore, in the temperature interval 25–60 °C the linear fit to the data gave a temperature coefficient of  $-45 \text{ K}^{-1}$ , which is larger in magnitude compared to those of LGP67, LGP68, and LGP68+, that is, copolymers nominally based on PPO of molecular weight 2000.<sup>3b</sup> Upon a further increase in temperature to 70 °C,  $N_{\text{agg}}$  was found to increase.

Owing to the negative temperature coefficient of solubility of the constituent blocks, the values of the aggregation number of the *Pluronic* copolymers as well as diblock PEO/PPO and di- and triblock PEO/PBO copolymers increase with increasing temperature.<sup>1h,12</sup> In that aspect, the behavior of the LGP copolymers of the present series is similar to that of the above-mentioned polyoxyalkylenes. However, in contrast to the latter, for which a gradual increase of  $N_{\text{agg}}$  with temperature has been found, for the present copolymers, maxima, breaks, and discontinuities are typically observed (Figure 6b). This indicates that the magnitude of  $N_{\text{agg}}$  or its variations with temperature is

governed by the superposition of two opposite processes: the increase in hydrophobicity of the PPO block, on one hand and the enhancement of the solubility of the PG moieties<sup>3a</sup> on the other. In other words, in strong contrast to *Pluronic* or other polyoxyalkylene block copolymers with increasing temperature the hydrophilic blocks of the LGP copolymers act completely oppositely to the PPO block. The exact value of  $N_{\text{agg}}$  at given temperature depends on the changeable balance between increasing both hydrophobicity of PPO and solubility of PG.

With regard to the magnitude of  $N_{\text{agg}}$ , the present copolymers can be broadly divided into aggregates with aggregation number below or slightly above 100 (LGP137 and LGP138) and aggregates with  $N_{\text{agg}}$  invariably well above 100 (LGP134 and LGP135). The latter two copolymers form particles relatively larger in aggregation number and size. It appeared that the density of the polymer material within the particle calculated as  $\rho = M_w/V$ , assuming a spherical shape and using the hydrodynamic radii to calculate the volume,  $V$ , is below 0.14 g·mL<sup>-1</sup>, which is typically lower than the densities of the rest of the copolymers studied (last column of Table 3). However, compared to those of the related LGP63–LGP68+ copolymers that form large compound particles,<sup>3b,c</sup> the self-assembled structures of LGP134 and LGP135 are denser and more compact. To gain information about the structure and morphology of the particles cryo-TEM was employed (Figure 7). Cryo-TEM is complementary to light scattering and is a technique for direct imaging of relatively large microstructures. Its resolution is about 4–5 nm; therefore, small core-corona polymeric micelles, as those that LGP136 at lower temperatures, LGP137, and LGP138 form, are typically observed as small black dots in the background.<sup>13</sup> Figure 7 shows micrographs taken from dispersions of LGP134 about 40 days after the initial preparation. In contrast to the close unilamellar vesicles observed in extruded aqueous solutions of *Pluronic* L121,<sup>14</sup> the structures in Figure 7 are compound and consist of two vesicles enclosed by a larger vesicle. The constituent vesicles seem to be distorted by pressing against each other, which is normally observed when small vesicles are enclosed by a larger one. The compound vesicles seem to contain a scattering material. The latter is outside the smaller constituent vesicles. The diameter of the compound vesicles is typically larger than 150 nm. Considering their peculiar structure, we may estimate that the radii of the constituent vesicles is about 30–40 nm, which is consistent with the DLS results (see Table 2). In some of the micrographs (not shown), dark globules, not too different from those encountered earlier,<sup>3b</sup> were observed. From the above facts we may hypothesize the formation of such compound vesicles. Initially, the constituent vesicles and the dark globules coexist; it is not known in what proportions since light scattering can not distinguish between them presumably because of the similarity in their dimensions. Due to the insufficient steric activity of PG and its ability to promote strong hydrogen bonding,<sup>3b</sup> these initial particles upon a prolonged period in close contact fuse together and eventually rearrange to form the compound vesicles shown in Figure 7. It can be noted that the lamellar structure of the particles is in good agreement with the relatively low  $\rho$  values.

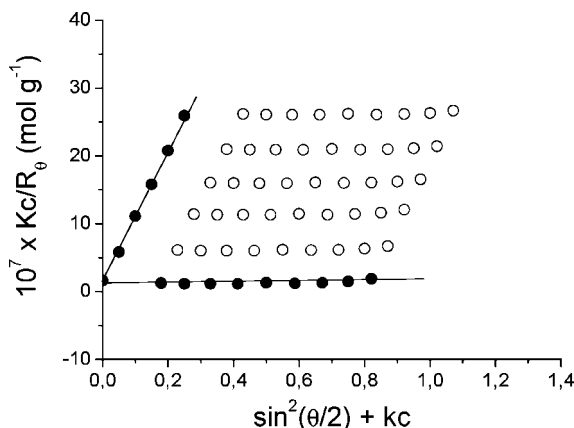
For LGP135 we were not able to visualize representative objects due to the limited time stability of its dispersions. Considering the experimental facts, we may suggest that it forms the same type of large compound particles consisting of discontinuous hydrophobic PPO domains randomly distributed in a strongly hydrogen-bonded continuous medium of PG and water, described earlier for related copolymers.<sup>3b,c</sup>

The density of the aggregates that LGP137 and LGP138 form at 25 °C is comparable to that of the aggregates of LGP134 and LGP135. With increasing temperature, however, the ag-

**Table 3. Static Light Scattering Parameters,  $R_g/R_h$  Ratios, and Density of Polymer Material within the Particles,  $\rho$ , of the Copolymers Studied in Water at Different Temperatures**

| copolymer, $T$ ( $^{\circ}\text{C}$ ) | $10^{-6} \times M_w$ ( $\text{g} \cdot \text{mol}^{-1}$ ) | $10^5 \times A_2$ ( $\text{mol} \cdot \text{mL} \cdot \text{g}^{-2}$ ) | $R_g$ (nm)        | $R_g/R_h$ | $\rho$ ( $\text{g} \cdot \text{mL}^{-1}$ ) |
|---------------------------------------|---|--|-------------------|-----------|--|
| LGP134, 25                            | 2.390   | 3.71   | 50.8              | 1.81      | 0.04                                       |
| 40                                    | 3.770   | -9.07  | 39.9              | 1.41      | 0.07                                       |
| 50                                    | 8.250   | -3.03  | 40.7              | 1.39      | 0.13                                       |
| 60                                    | 6.060   | -1.80  | 45.1              | 1.56      | 0.10                                       |
| 70                                    | 7.800   | -4.56  | 48.3              | 1.73      | 0.14                                       |
| LGP135, 25                            | 15.050  | 3.03   | 86.0              | 1.58      | 0.04                                       |
| 40                                    | 7.350   | -6.32  | 59.8              | 1.57      | 0.05                                       |
| 50                                    | 4.040   | -5.65  | 57.6              | 1.50      | 0.03                                       |
| 60                                    | 4.320   | -5.70  | 56.7              | 1.47      | 0.03                                       |
| 70                                    | 6.840   | -4.31  | 50.6              | 1.50      | 0.07                                       |
| LGP136, 25                            | 1.850   | 22.9   |                   |           | 0.25                                       |
| 40                                    | 2.830   | 15.1   |                   |           | 0.48                                       |
| 50                                    | 3.570   | 15.3   |                   |           | 0.57                                       |
| 60                                    | 9.180   | 13.3   | 62.0              | 2.64      | <sup>b</sup>                               |
| 70                                    | 23.750  | 21.8   | 103.2             | 3.21      | <sup>b</sup>                               |
| LGP137, 25                            | 0.650   | 0.735  | 25.9 <sup>a</sup> | 1.69      | 0.07                                       |
| 40                                    | 1.240   | 2.76   | 15.8 <sup>a</sup> | 1.31      | 0.28                                       |
| 50                                    | 1.880   | 2.06   | 13.3 <sup>a</sup> | 1.10      | 0.42                                       |
| 60                                    | 1.690   | 4.38   | 12.6 <sup>a</sup> | 1.01      | 0.34                                       |
| 70                                    | 2.540   | 3.47   | 12.7 <sup>a</sup> | 1.02      | 0.53                                       |
| LGP138, 25                            | 0.860   | 1.28   | 35.3 <sup>a</sup> | 1.88      | 0.05                                       |
| 40                                    | 1.280   | 2.96   | 17.0 <sup>a</sup> | 1.33      | 0.24                                       |
| 50                                    | 1.420   | 3.16   | 18.7 <sup>a</sup> | 1.43      | 0.25                                       |
| 60                                    | 1.000   | 0.80   | 18.7 <sup>a</sup> | 1.34      | 0.14                                       |
| 70                                    | 0.940   | -1.45  | 24.0 <sup>a</sup> | 1.78      | 0.15                                       |

<sup>a</sup> Apparent radius of gyration,  $R_g^{\text{app}}$ , determined from partial Zimm plot. <sup>b</sup> Not applicable.

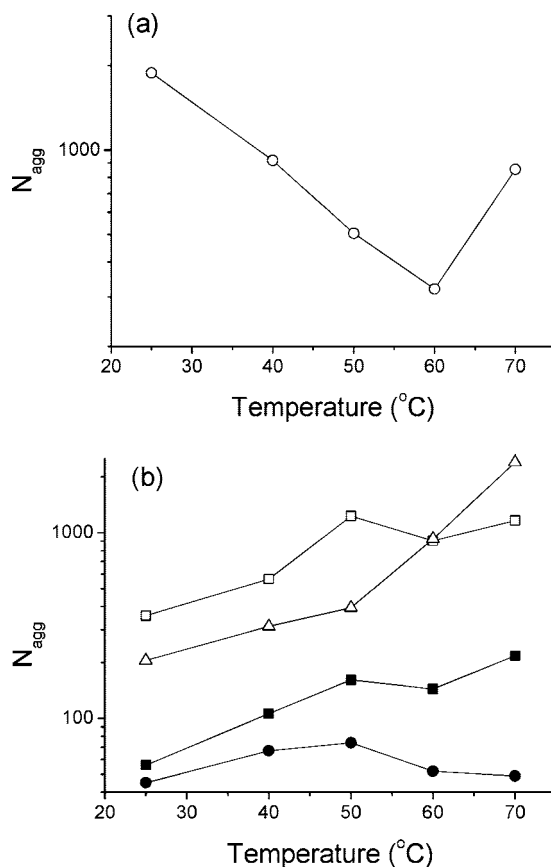


**Figure 5.** Zimm plot of LGP134 in water at 60  $^{\circ}\text{C}$ : experimental points (open symbols); extrapolated to zero aggregate concentration and zero scattering angle points (closed symbols).

gregates became more compact and denser. This finding can be easily related to the increasing hydrophobicity of PPO. Obviously, the latter dominates over the increasing solubility of the PG moieties, though the two processes superimpose, which is also reflected by the variations in  $\rho$  with temperature. In that aspect, the  $\rho$  values for the aggregates of LGP136, which at a given temperature are invariably higher than those of LGP137 and LGP138 and are consistent considering the copolymer composition and particle structure. At 60 and 70  $^{\circ}\text{C}$ ,  $\rho$  was not determined because of the transition to nonspherical particles.

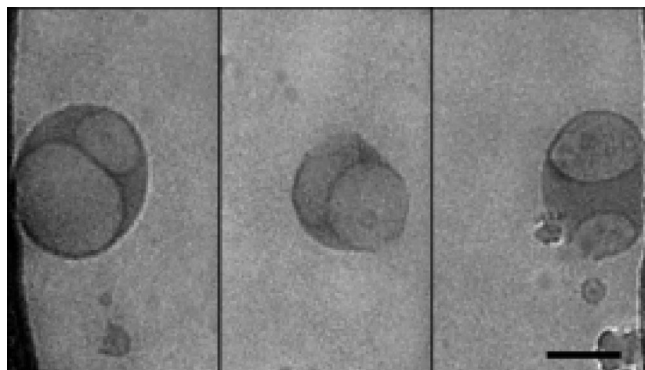
#### Small-Angle Neutron Scattering Experiments. LGP135.

We start this section with LGP135 because of the similarities between its behavior and those of the related copolymers studied earlier.<sup>3c</sup> As pointed out in the previous section, the particles that LGP135 forms are smaller in size and aggregation number and more compact than the large compound particles formed by LGP63–LGP68+.<sup>3c</sup> Figure 8 shows representative scattering profiles of a solution of LGP135 with a concentration of 2 wt % at 25, 40, 50, and 60  $^{\circ}\text{C}$ . The data were analyzed by slope determination. For this copolymer, no scattering from large

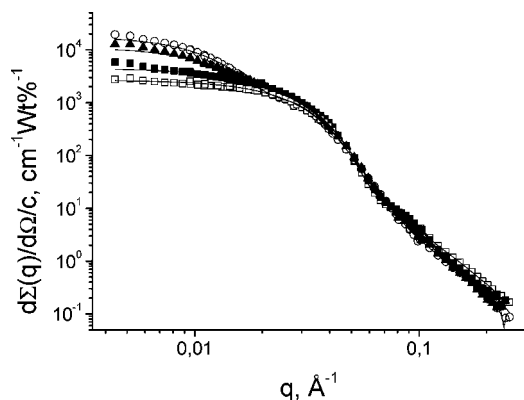


**Figure 6.** Temperature dependence of the aggregation number,  $N_{\text{agg}}$ , of LGP135 (a) and LGP134 (open squares), LGP136 (open triangles), LGP137 (closed squares), and LGP138 (closed circles) in (b). The lines through the data points are a guide for the eye.

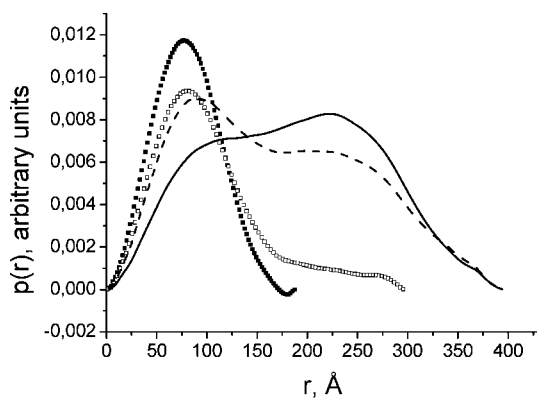
(> 100 nm) particles was detected, which is in good agreement with the DLS results, showing  $R_h$  was invariably below 54.6 nm (Table 2). On the  $q$  scale of the SANS measurements and considering the size of the particles that LGP135 forms, the scattering objects (presumably PPO domains) can be considered



**Figure 7.** Cryo-TEM micrographs of samples taken from aqueous dispersions of LGP134. The bar length is 100 nm.



**Figure 8.** SANS data for a 2 wt % solution in D<sub>2</sub>O of LGP135 at 25 (open squares), 40 (closed squares), 50 (triangles), and 60 (circles) °C, together with fits of IFT analysis (solid lines).



**Figure 9.** Pair distance distribution function,  $p(r)$ , obtained from the SANS data of a 2 wt % solution of LGP135 in D<sub>2</sub>O at 25 (closed squares), 40 (open squares), 50 (dashed line), and 60 (solid line) °C.

as individual entities in the interior of the large particles. Another feature is the absence of scattering from nonassociated Gaussian chains in strong contrast from the copolymers of the previous series,<sup>3c</sup> which implies that all copolymer chains self-associate.

The scattering curves were converted into real space equivalents, pair distance distribution function,  $p(r)$ , which was done by an indirect Fourier transformation (IFT) procedure developed by Glatter.<sup>15</sup> Figure 9 shows the evolution of the  $p(r)$  function with temperature for the dilute solution of LGP135. At 25 °C, the  $p(r)$  function is close to symmetrical, implying that the domains are almost spheres. At temperatures  $\geq 40$  °C, a shoulder and a second maximum, which became dominant on further heating, appeared. The appearance of a shoulder/additional maximum is usually an indication for scattering from the corona

**Table 4.** Values of Finite Maximal Dimensions of the Domains ( $D_{\max}$ ), Major Semi-Axis,  $a$ , and Semi-Axis Ratios,  $\mu$ , for Dilute (2 wt %) Aqueous Solution of Selected Copolymers at Different Temperatures

| copolymer, $T$ (°C) | $D_{\max}$ (nm) | $a$ (nm)     | $\mu$          |
|---------------------|-----------------|--------------|----------------|
| LGP135, 25          | 19.0            | 8.5          | 0.67           |
| 40                  | 30.0            | <sup>a</sup> | <sup>a</sup>   |
| 50                  | 40.0            | <sup>a</sup> | <sup>a</sup>   |
| 60                  | 40.0            | <sup>a</sup> | <sup>a</sup>   |
| LGP136, 25          | 20.0            | 9.4          | $0.64 \pm 0.1$ |
| 40                  | 20.0            | 9.4          | $0.70 \pm 0.1$ |
| 50                  | 20.0            | 9.5          | $0.72 \pm 0.1$ |
| 60                  | 21.0            | 9.8          | $0.72 \pm 0.1$ |
| LGP138, 25          | 19.0            | 9.5          | $0.71 \pm 0.2$ |
| 40                  | 19.0            | 9.5          | $0.77 \pm 0.2$ |
| 50                  | 19.0            | 9.5          | $0.77 \pm 0.2$ |
| 60                  | 20.0            | 10.0         | $0.77 \pm 0.2$ |

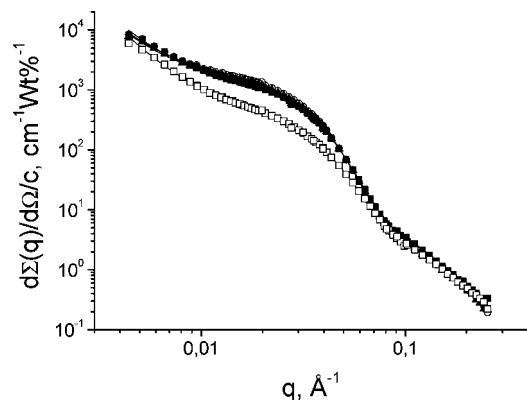
<sup>a</sup> Not determined.

that is getting more compact. However, the particles of LGP135 can not be modeled as simple core-corona particles, and consequently, we can suggest coexistence of objects of different morphologies at elevated temperatures. Thus, the almost spherical PPO domains that are observed at 25 °C exist also at elevated temperatures. A fraction of domains of different morphology is formed at  $\geq 40$  °C, and the two kinds of objects coexist. Strictly speaking, the dominant objects at lower temperatures probably also undergo a shape transformation, judged by the slight shift of the position of the maximum with increasing temperature; as shown by King,<sup>16</sup> the shapes and, in particular, the positions of maxima of the  $p(r)$  functions are different for spheres, prolate ellipsoids, and oblate ellipsoids having the same radius of gyration,  $r_g$ , values. At that stage of the investigations we do not know anything about the morphology of the accompanying domains; what is clear, however, is that the transition is broad and retarded most probably due to the slow kinetics associated with the peculiar structure of the large particles discussed elsewhere.<sup>3b</sup>

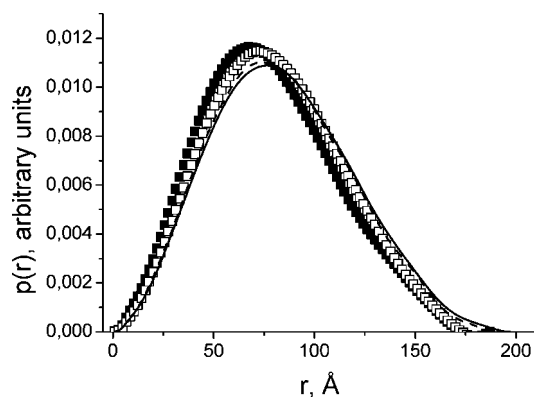
The  $r_g$  values were determined from the second moment of the  $p(r)$  distribution functions. The domains are relatively small ( $r_g = 6.2$  nm) at 25 °C and gradually increase with increasing temperature, reaching 14.5 nm at 60 °C. It should be noted, however, that the radii of gyration at elevated temperatures represent averaged values between  $r_g$  of domains of presumably different morphologies and dimensions. The scattering data were fitted to a model of ellipsoids of revolution with excluded volume interactions. The results for the semiaxis,  $a$ , and the semiaxis ratio,  $\mu$ , at 25 °C are presented in Table 4. The model fitting at elevated temperatures did not give reasonable results most probably due to coexistence of PPO domains of different shapes.

**LGP136, LGP137, and LGP138.** The particles that these three copolymers form in dilute aqueous solution are, as deduced from light scattering, of the familiar core-corona spherical structure. Only for LGP136 at temperatures  $\geq 60$  °C a sharp increase in particle dimensions and  $R_g/R_h$  ratio was observed (Tables 2 and 3), implying formation of elongated particles. The scattering profiles of LGP138 (Figure 10) are somewhat different from those of LGP135 in that at the lowest  $q$  traces of scattering from large particles are seen (slope  $\approx 2.8$ ). As noted in the LS section, a small fraction of large particles, that was removed following filtration coexisted with the dominant core-corona micelles. The solutions for SANS, however, were not filtered. Nevertheless, because the scattering objects under investigation by SANS (PPO domains) are the same for the micelles and large compound particles, the coexistence of the former and the latter is not expected to twist the results. Scattering from large particles was detected for LGP137 as well.

The almost symmetrical and bell-like shapes of the  $p(r)$  functions observed for the three copolymers at all temperatures



**Figure 10.** SANS data for a 2 wt % solution in D<sub>2</sub>O of LGP138 at 25 (open squares), 40 (closed squares), 50 (triangles), and 60 (circles) °C together with fits of IFT analysis (solid lines). The slopes at the lowest  $q$  range are close to 2.8, indicating scattering from large (above 100 nm) particles.



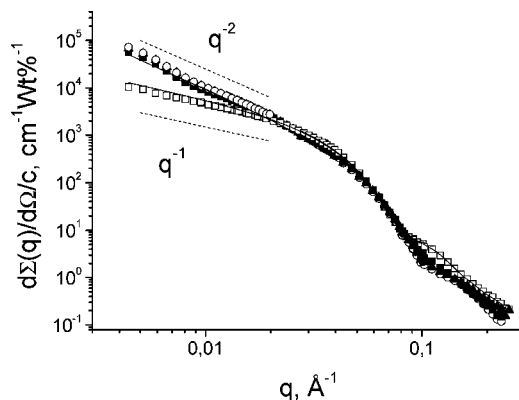
**Figure 11.** Pair distance distribution function,  $p(r)$ , obtained from the SANS data of a 2 wt % solution of LGP136 in D<sub>2</sub>O at 25 (closed squares), 40 (open squares), 50 (dashed line), and 60 (solid line) °C.

**Table 5.** Radii of Gyration ( $r_g$ ) of the PPO Domains, the Corresponding Radii of Equivalent Spheres ( $r$ ), and Corona Thickness ( $\delta$ ) of the Core-Corona Particles Formed in Dilute Aqueous Solution by LGP136, LGP137, and LGP138 at Various Temperatures

| system         | $r_g$ (nm) | $r$ (nm) | $\delta$ (nm) |
|----------------|------------|----------|---------------|
| LGP136, 2 wt % |            |          |               |
| 25 °C          | 6.7        | 8.6      | 5.8           |
| 40 °C          | 6.9        | 8.9      | 4.4           |
| 50 °C          | 7.0        | 9.0      | 4.5           |
| 60 °C          | 7.2        | 9.3      |               |
| LGP137, 2 wt % |            |          |               |
| 25 °C          | 6.5        | 8.4      | 6.9           |
| LGP138, 2 wt % |            |          |               |
| 25 °C          | 5.9        | 7.6      | 11.2          |
| 40 °C          | 6.1        | 7.9      | 4.2           |
| 50 °C          | 6.4        | 8.3      | 4.8           |
| 60 °C          | 6.5        | 8.4      | 5.6           |

strongly contrasted those of LGP135 (cf. Figures 9 and 11). The  $r_g$  values for LGP136 and LGP138 were found to gradually increase with increasing temperature by 7–10% (Table 5). Unfortunately, no reliable data were obtained for LGP137 due to uncertainty in the solute concentration. The  $r_g$  values are somewhat smaller for LGP138 and increase with decreasing PG content. Obviously, the mechanism by which the lateral pressure between the longer PG chains in coronae is relaxed involves curving of the domain surface through formation of domains of smaller  $r_g$ .

When the results from DLS and SANS were combined, it was possible to estimate the corona thickness,  $\delta$ . The latter was



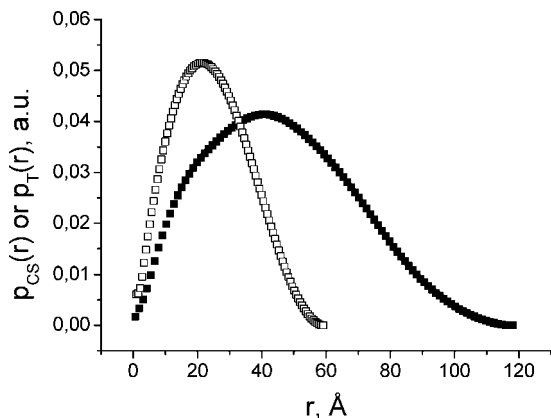
**Figure 12.** SANS data for a 2 wt % solution in D<sub>2</sub>O of LGP134 at 25 (open squares), 40 (closed squares), 50 (triangles), and 60 (circles) °C together with fits of IFT analysis (solid lines).

calculated as difference between the hydrodynamic radii from DLS and the radii of the equivalent sphere,  $r = (5/3)^{1/2} r_g$ , from SANS. The radii of the equivalent sphere corresponded to the radii of the PPO domains since the latter made the major contribution to the scattering due to the large differences in the scattering length densities of PPO and PG. The results presented in Table 5 indicate that in the temperature interval 40–60 °C the thicknesses are either stable (LGP136) or gradually increase upon heating (LGP138). Somewhat surprising are the similar values of  $\delta$  in that temperature interval for the micelles of LGP136 and LGP138 though the two copolymers differ considerably in PG chain length. This finding can be rationalized in terms of different stretching of the PG chains in the corona. Thus, the PG chains in the coronae of the LGP136 micelles are more stretched because of the lower curvature (larger dimensions) of the PPO domains. Less stretched are the PG chains of the coronas of LGP138 micelles due to the more curved surface on which they are grafted. Somewhat puzzling are the large values of corona thickness observed at 25 °C. It has been shown previously<sup>17</sup> that water at 25 °C provides for PG worse solvent conditions than for PEO and that PG tends to adopt elongated coil conformation. Such a conformation may be responsible for the larger micellar dimensions (Table 2) and, consequently, corona thicknesses (Table 5) observed at 25 °C.

Similar to the PPO domains of the aggregates of LGP135, those of LGP136, LGP137, and LGP138 are slightly anisotropic at lower temperatures. Heating leads to an increase of the smaller semiaxis,  $b$ , and, consequently,  $\mu$  (Table 4). In other words, the PPO domains become more spherical at elevated temperatures in a dissimilar fashion not only to LGP135 but also for some Pluronic copolymers for which sphere-to-rod transition is typically observed upon increasing temperature.<sup>1e,18</sup> Such a behavior is to be expected considering the high contents of PG and its “normal” solubility in water. It is noteworthy also that the SANS data for LGP136 at 60 °C do not evidence structural changes in contrast to LS. This discrepancy may indicate that the transition in D<sub>2</sub>O is shifted toward higher temperatures and thus is located beyond the upper temperature limit of the SANS experiments.

**LGP134.** Figure 12 shows the scattering profiles of a 2 wt % solution of LGP134 in D<sub>2</sub>O at different temperatures. The slopes in the low  $q$  range ( $q < 0.01$  Å<sup>−1</sup>) are around −1 and −2 at 25 °C and  $\geq 40$  °C, respectively, suggesting a rod-to-lamella transition upon heating. Whereas the lamellar organization at  $\geq 40$  °C is consistent with the LS and cryo-TEM studies, the data at 25 °C is not: the LS parameters (Tables 2 and 3) do not indicate formation of elongated one-dimensional structures. The reason for this discrepancy could be if we assume that the aggregates at 25 °C are worm-like and flexible with dimensions





**Figure 13.** Pair distance distribution function of cylindrical cross section  $p_{CS}(r)$  obtained from the SANS data of 2 wt % solution of LGP134 in  $D_2O$  at 25 °C (filled squares) and pair distance distribution function of thickness of vesicles  $p_T(r)$  obtained from the SANS data of 2 wt % solution of LGP134 in  $D_2O$  at 40 °C (empty squares).

that coincide with the dimensions of the vesicles at elevated temperatures. The model fitting, however, does not support such structures. Alternatively, we must admit that the rod-to-lamella transition in  $D_2O$  is shifted toward higher temperatures. In other words, at 25 °C in  $H_2O$  (results from LS) the above transition has already taken place, whereas in  $D_2O$  it is at temperatures between 25 and 40 °C.

The data in the large  $q$  range ( $q > 0.01 \text{ Å}^{-1}$ ) were analyzed using the IFT method assuming rod-like geometry at 25 °C. The scattering intensities for rod-like aggregates can be expressed via the cross-section pair distance distribution function  $p_{CS}(r)$

$$d\Sigma(q)/d\Omega = \left(\frac{\pi}{q}\right) 2\pi \int_0^\infty p_{CS}(r) J_0(qr) dr \quad (5)$$

where  $J_0$  is the zeroth-order Bessel function.

The  $p_{CS}(r)$  function is given by<sup>15</sup>

$$p_{CS}(r) = \frac{c}{2\pi M_L} \int r \Delta\rho(\mathbf{r}') \Delta\rho(\mathbf{r} + \mathbf{r}') d\mathbf{r}' \quad (6)$$

where  $\Delta\rho(r)$  is the contrast (difference between the scattering length density of aggregates at the point  $r$ ,  $\rho(r)$ , and the averaged scattering length density of the solvent  $\rho_s$ ,  $\Delta\rho(r) = \rho(r) - \rho_s$ , and the vectors  $\mathbf{r}$  and  $\mathbf{r}'$  are lying in the cross-section plane. The pair distance distribution function is expressed as a sum of  $N$  b-splines evenly distributed in the interval  $[0, D_{\max}]$ . The values of the coefficients are calculated numerically by least-squares fitting of the IFT model curve to the experimental data. In the present study, the values of  $D_{\max}$  were carefully selected to give both good fits to the experimental data and smooth  $p_{CS}(r)$  functions. The Gaussian shape of the pair distribution function (Figure 13) is characteristic for almost homogeneous cylindrical aggregates. The first estimation of the cross-section diameter of about 12 nm was obtained from the maximum distance of  $p_{CS}(r)$ . Furthermore, the radius of gyration of the cross section,  $r_{CS,g}$ , the radius of the homogeneous circular cross section,  $r_C$ , as well as the mass per unit length of the aggregate,  $M_L$ , and the surface area occupied by one LGP134 macromolecule were determined. All parameters are collected in Table 6.

The data at elevated temperatures at which scattering from aggregates of lamellar structure (vesicles) was observed ( $d\Sigma(q)/d\Omega \sim q^{-2}$  in Figure 12), were analyzed by IFT assuming disk-like geometry; because the radius of the vesicle is much larger than the thickness of the lamella the scattering can be modeled as scattering from anisotropic, two-dimensional, flat objects (disks). In that case the scattering intensities can be

**Table 6.** Parameters Fitted to the SANS Data of a 2 wt % Solution of LGP134 in  $D_2O$  at Different Temperatures

| parameter   | rod-like morphology at 25 °C | vesicles at temperatures $\geq 40$ °C |
|---|------------------------------|---------------------------------------|
| $D_{\max}$ (nm)   | 12.0                         | 6.0                                   |
| $r_{CS,g}$ (nm) radius of gyration of the cross section   | 3.8                          |                                       |
| $r_C$ (nm) radius of the homogeneous circular cross section   | 5.3                          |                                       |
| $10^{13} \times M_L$ ( $\text{g} \cdot \text{cm}^{-1}$ ) mass per unit length of the aggregate          | 5.74                         |                                       |
| $r_{T,g}$ (nm) radius of gyration of thickness  |                              | 1.9                                   |
| $r_T$ (nm) thickness of a homogeneous disk-like aggregate   |                              | 6.5                                   |
| $10^{10} \times M_S$ ( $\text{g} \cdot \text{cm}^{-2}$ ) mass per surface area of a disk-like aggregate |                              | 5.65                                  |
| surface area per macromolecule ( $\text{nm}^2$ )  | 6.4                          | 4.0                                   |

presented in the form of the thickness pair distance distribution function  $p_T(r)$  (eq 7)

$$d\Sigma(q)/d\Omega = \left(\frac{2\pi}{q^2}\right) \pi \int_0^\infty p_T(r) \cos(qr) dr \quad (7)$$

The  $p_T(r)$  function is given by eq 8<sup>15</sup>

$$p_T(r) = \frac{c}{2\pi M_S} \int \Delta\rho(r') \Delta\rho(r + r') dr' \quad (8)$$




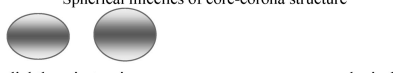
Here,  $r$  is the coordinate in the  $x$ -direction and  $M_S$  corresponds to the mass per surface units of disk-like aggregates (vesicles). An example of the pair distance distribution function of thickness of vesicle walls  $p_T(r)$  obtained at 40 °C is shown in Figure 13. Related parameters were extracted and presented in Table 6. The results at 50 and 60 °C are very close (within the experimental error) to those at 40 °C and, therefore, are not presented.

Although the rod-like and vesicular morphologies of the aggregates of *Pluronic* copolymers are well-documented, the literature contains surprisingly very few results of the values of the radius of the rod-like particles and the thickness of the lamella that can be compared with those for the aggregates of LGP134.<sup>19</sup> Possible reasons could be that the research on copolymers that form particles of such morphologies and the conditions at which these morphologies are typically observed (high temperatures, high concentrations, presence of cosolutes and/or salts) are largely neglected. Although not directly comparable the results obtained for LGP134 are in good agreement with those of the *Pluronic* analogues. It should be noted as well that the decrease of the surface area per one LGP134 macromolecule (last row of Table 6) is consistent with the rod-to lamella transition suggested above.

## Concluding Remarks

The copolymers of the present series exhibit undoubtedly richer structural polymorphism compared to the related copolymers nominally based on PPO 2000.<sup>3b,c</sup> The latter form large compound particles in the interior of which slightly prolate PPO domains coexist with nonassociated copolymer chains.<sup>3c</sup> In some aspects the aggregates of LGP135 resemble them, but they are denser, more compact, and do not contain nonassociated copolymer chains, which is compatible with the longer and, consequently, more hydrophobic PPO block. The rest of the copolymers investigated in the present study form in aqueous solution a variety of nanosized particles including core-corona micelles, vesicles, and particles of rod-like morphology. The structural polymorphism and the shape transitions with temperature and copolymer composition are presented in Figure 14. The copolymers of relatively long PG chains (PG content



| Copolymers        | Transitions   | Notes   |
|-------------------|---|---|
| LGP134            | <br>rod      vesicle                           | Transition detected by SANS                                       |
| LGP135            | <br>slightly anisotropic      more anisotropic | Co-existence of domains of different morphologies at $\geq 40$ °C |
| LGP136            | <br>slightly anisotropic      more spherical   | Transition to rod-like morphology according to LS at $\geq 60$ °C |
| LGP137 and LGP138 | <br>slightly anisotropic      more spherical   | The aggregates that LGP137 and LGP138 form are identical          |
|                   | 25      40      50      60      70  | Temperature (°C)  |

**Figure 14.** Shape transitions of PPO domains with temperature and copolymer composition. The objects are not drawn to scale.

$\geq 60$  wt %) form micelles of practically spherical core-corona structure, whereas particles of vesicular and cylindrical organizations are observed for LGP134. Basically, the sequence of morphologies, that is, more spherical, slightly anisotropic, more anisotropic, and lamellar (vesicular) is analogous to that observed for other amphiphilic block copolymers (cf. the sphere-rod-lamella transition upon decreasing hydrophilic-to-hydrophobic ratio for *Pluronic* copolymers<sup>1c</sup>). This sequence is more distinctively pronounced at elevated temperatures (Figure 14).

$N_{\text{agg}}$  of *Pluronic* micelles is known to increase with increasing temperature, whereas the dimensions are mostly insensitive to temperature due to compensation effects between an increase in  $N_{\text{agg}}$  and a decrease in coronal swelling. Upon increasing  $N_{\text{agg}}$ , the diameter of the micellar core may become comparable to the length of the fully stretched PPO block, which is considered responsible for the shape transitions from spheres to prolate ellipsoids and rods.<sup>18a</sup> Similarly, the temperature variations in the dimensions of the aggregates of the present LGP copolymers are only slightly pronounced. However, upon heating the simultaneous increase of hydrophobicity of PPO and hydrophilicity of PG counteract, which imparts maxima and discontinuities in the temperature dependence of  $N_{\text{agg}}$  (Figure 6b). That is why, besides the “normal”, that is, sphere-rod and eventually lamella, thermotropic transition [for the present copolymers it corresponds to sphere-rod (LGP136), rod-vesicle (LGP134), slightly anisotropic-more anisotropic (LGP135)], an anomalous sequence (slightly anisotropic-more spherical) is observed for some of the copolymers (Figure 14).

Although the PPO domains of the micelles of the copolymers of higher PG content especially at lower temperatures can be of morphology somewhat deviating from the spherical one, the light scattering results do not evidence that the micelles are not spherical, which may imply that the anisotropy of the PPO domains is compensated by the bulky PG chains in the corona. The seeming disagreements between the SANS and LS results can be rationalized in terms of shift of transitions to higher temperatures when D<sub>2</sub>O is the dispersion medium. This finding is in line with the behavior of short-chain nonionic surfactants and contrasts that of the *Pluronic* copolymers,<sup>18c</sup> which demonstrates once again the empirical and system-specific character of the deuterium substitution.<sup>16</sup>

**Acknowledgment.** The financial support of COST programme (COST-STSM-P12-02727) is gratefully acknowledged. The

SANS study was supported by the European Commission under the 6th Framework Programme through the Key Action: Strengthening the European Research Area, Research Infrastructures (Contract RII3-CT-2003-505925). We thank G. Karlsson, Department of Physical and Analytical Chemistry, University of Uppsala, Sweden for helping us with the electron microscopy.

**Supporting Information Available:** Estimation of the relative concentrations of the particles responsible for the slow and fast modes. The information is available free of charge via the Internet at <http://pubs.acs.org>.

## References and Notes

- (1) (a) Lunsted, L. G.; Schmolka, I. R. In *Block and Graft Copolymers*; Ceresa, R. J., Ed.; John Wiley: New York, 1976. (b) Schmolka, I. R. In *Polymers for Controlled Drug Delivery*; Tarcha, P. J., Ed.; CRC Press: Boca Raton, Ann Arbor, Boston, 1991. (c) Wanka, G.; Hoffmann, H.; Ulbricht, W. *Macromolecules* **1994**, *27*, 4145. (d) Alexandridis, P.; Hatton, T. A. *Colloid Surf., A* **1995**, *96*, 1–46. (e) Almgren, M.; Brown, W.; Hvídt, S. *Colloid Polym. Sci.* **1995**, *273*, 2. (f) Chu, B. *Langmuir* **1995**, *11*, 414–21. (g) Mortensen, K. *J. Phys.: Condens. Matter* **1996**, *8*, A103. (h) Chu, B.; Zhou, Z.-K. In *Nonionic Surfactants, Poly(oxyalkylene) Block Copolymers, Surfactant Science Series*; Nace, V. M., Ed.; Marcel Dekker: New York, 1996. (i) Alexandridis, P. *Curr. Opin. Colloid Interface Sci.* **1997**, *2*, 478. (j) Hamley, I. W. *The Physics of Block Copolymers*, Oxford University Press: New York, 1998. (k) Alexandridis, P.; Lindman, B. *Amphiphilic Block Copolymers: Self-Assembly and Application*; Elsevier: Amsterdam, 2000.
- (2) Strictly speaking, PPO and PBO are materials exhibiting lower critical solution temperature (LCST) properties, which means that they are not truly hydrophobic, but hydrophobic at certain (elevated temperatures) conditions.
- (3) (a) Halacheva, S.; Rangelov, S.; Tsvetanov, Ch. *Macromolecules* **2006**, *39*, 6845–52. (b) Rangelov, S.; Almgren, M.; Halacheva, S.; Tsvetanov, Ch. *J. Phys. Chem. C* **2007**, *111*, 13185–91. (c) Halacheva, S.; Rangelov, S.; Haramus, V. *Macromolecules* **2007**, *40*, 8015–21.
- (4) Halacheva, S.; Rangelov, S.; Tsvetanov, Ch. *Macromolecules* **2008**, *41*, 7699–705.
- (5) Rangelov, S.; Brown, W. *Polymer* **2000**, *41*, 4825–30.
- (6) Chu, B. *Laser Light Scattering*, 2nd edition; Academic Press: New York, 1991.
- (7) Jakes, J. *Czech J. Phys. B* **1988**, *38*, 1305–16.
- (8) Stuhmann, H. B.; Burkhardt, N.; Dietrich, G.; Junemann, R.; Meerwinck, W.; Schmitt, M.; Wadzak, J.; Willumeit, R.; Zhao, J.; Nierhaus, K. H. *Nucl. Instrum. Methods* **1995**, *A356*, 133.
- (9) Pedersen, J. S.; Posselt, D.; Mortensen, K. *J. Appl. Crystallogr.* **1990**, *23*, 321.
- (10) Rangelov, S.; Halacheva, S.; Tsvetanov, Ch. Manuscript in preparation.
- (11) (a) Burchard, W. *Adv. Polym. Sci.* **1983**, *48*, 1. (b) Thurn, A.; Burchard, W.; Niki, R. *Colloid Polym. Sci.* **1987**, *265*, 653.
- (12) (a) Booth, C.; Yu, G.-E.; Nace, V. M. In *Amphiphilic Block Copolymers: Self-Assembly and Applications*; Alexandridis, P.; Lindman, B., Eds.; Elsevier Science: New York, 2000. (b) Booth, C.; Attwood, D. *Macromol. Rapid Commun.* **2000**, *21*, 501. (c) Yu, G.-E.; Yang, Z.; Ameri, M.; Attwood, D.; Collett, J. H.; Price, C.; Booth, C. *J. Phys. Chem. B* **1997**, *101*, 4394–401. (d) Altinok, H.; Nixon, S. K.; Gorry, P. A.; Attwood, D.; Booth, C.; Kelarakis, A.; Havredaki, V. *Colloids Surf., B* **1999**, *16*, 73–91. (e) Yu, G.-E.; Li, H.; Price, C.; Booth, C. *Langmuir* **2002**, *18*, 7756–8. (f) Liu, T.; Zhou, Z.; Wu, C.; Nace, V. M.; Chu, B. *J. Phys. Chem. B* **1998**, *102*, 2875–82.
- (13) (a) Almgren, M.; Edwards, K.; Karlsson, G. *Colloid Interface Sci., A* **2000**, *174*, 3–21. (b) Edwards, K.; Johansson, M.; Karlsson, G.; Silander, M. *Biophys. J.* **1997**, *73*, 258–66. (c) Rangelov, S.; Almgren, M.; Tsvetanov, Ch.; Edwards, K. *Macromolecules* **2002**, *35*, 7074–81.
- (14) Schillen, K.; Bryskhe, K.; Málnikova, Y. *Macromolecules* **1999**, *32*, 6885–8.
- (15) Glatter, O. *J. Appl. Crystallogr.* **1977**, *10*, 415–21.
- (16) King, S. M. Small-Angle Neutron Scattering. In *Modern Techniques for Polymer Characterization*; Pethrick, R. A., Dawkins, J. V., Eds.; John Wiley & Sons, Ltd.: New York, 1999; Chapter 7.
- (17) Rangelov, S.; Trzebiecka, B.; Jamroz-Piega, M.; Dworak, A. *J. Phys. Chem. B* **2007**, *111*, 11127–33.
- (18) (a) Mortensen, K.; Pedersen, J. S. *Macromolecules* **1993**, *26*, 805–12. (b) Glatter, O.; Scherf, G.; Schillen, K.; Brown, W. *Macromol-*

ecules **1994**, 27, 6046–54. (c) King, S. M.; Heenan, R. K.; Cloke, V. M.; Washington, C. *Macromolecules* **1997**, 30, 6215–22. (d) Schillen, K.; Brown, W.; Johnsen, R. *Macromolecules* **1994**, 27, 4825–32. (e) Jorgensen, E. B.; Hvidt, S.; Brown, W.; Schillen, K. *Macromolecules* **1997**, 30, 2355–64. (f) Al-saden, A. A.; Whately, T. L.; Florence, A. T. *J. Colloid Interface Sci.* **1982**, 90, 303–9. (g) Mortensen, K.; Brown, W. *Macromolecules* **1993**, 26, 4128–35.

(19) (a) Hecht, E.; Mortensen, K.; Hoffmann, H. *Macromolecules* **1995**, 28, 5465–76. (b) Ganguly, R.; Aswal, V. K.; Hassan, P. A.; Gopalakrishnan, I. K.; Yakhmi, J. V. *Pramana* **2004**, 63, 277–83. (c) Zipfel, J.; Berghausen, J.; Schmidt, G.; Lindner, P.; Alexandridis, P.; Richering, W. *Macromolecules* **2002**, 35, 4064–74.

MA801238X